Journal of Catalysis **190,** 182–190 (2000)
doi:10.1006/jcat.1999.2731, available online at http://www.idealibrary.com on IDEAL®

Morphology of Rhodium Particles in Ex-chloride $Rh/Ce_{0.5}Zr_{0.5}O_2$ Catalyst

G. Vlaic,*,† P. Fornasiero,* G. Martra,* E. Fonda,* J. Kašpar,*,[1] L. Marchese,‡ E. Tomat,* S. Coluccia,* and M. Graziani*

*Dipartimento di Scienze Chimiche, Università di Trieste, Via Giorgieri 1, 34127 Trieste, Italy; †Experimental Division, Sincrotrone Trieste S.p.A., Padriciano, Trieste, Italy; and ‡Dipartimento di Scienze e Tecnologie Avanzate, Università del Piemonte Orientale "A. Avogadro", C.so Borsalino 54, I-15100, Alessandria, Italy

Received August 4, 1999; revised October 7, 1999; accepted October 9, 1999

The morphologyof rhodium particles in a 5 wt% $Rh/Ce_{0.5}Zr_{0.5}O_2$ catalyst subjected to different treatments is investigated by EXAFS, HREM, and H_2 chemisorption. Despite the high Rh loading, highly dispersed metal particles are observed in the sample. In the presence of NO and CO, the Rh particles are easily oxidized to give small Rh oxide clusters, and the high rhodium dispersion is retained even after a further reduction at 773 K. Comparison with an Rh/Al_2O_3 prepared under identical conditions clearly suggests that the presence of the $Ce_{0.5}Zr_{0.5}O_2$ support favors high dispersion of rhodium particles. Despite the fact that $RhCl_3 \cdot nH_2O$ has been employed as precursor, no chloride could be detected in the Rh nearest-neighbor shell, suggesting its migration over the support.

Key Words: **rhodium catalysts; ceria–zirconia mixed oxides; Rh/CeO_2–ZrO_2 solid solutions; rhodium chloride; Rh catalysts, EXAFS analysis of; three-way catalysts.**

1. INTRODUCTION

State-of-the-art automotive three-way catalysts (TWCs) nowadays contain ceria–zirconia mixed oxides due to their high efficiency in promoting the so-called oxygen storage capacity (OSC) and their high thermal stability (1). OSC is the ability of CeO_2-based promoters to act as an oxygen buffer under exhaust conditions by releasing/acquiring oxygen through redox processes involving the Ce^{4+}/Ce^{3+} couple. In addition, CeO_2 has been known to promote a variety of noble metal (NM)–CeO_2 interactions, resulting in highly efficient TWCs (2). In a previous paper we investigated the effects of CeO_2–ZrO_2 mixed oxides on the reduction of NO with CO and disclosed a promotional effect of the support upon the activity of rhodium (3). In addition, IR evidence for an active role of the CeO_2–ZrO_2 mixed oxides in stabilizing high dispersion of the rhodium particles was reported since in the presence of CO the gem-Rh^I-dicarbonyl was observed up to 523 K and no reductive agglomeration of Rh particles could be detected (3). This was an interesting observation since it is well known that above approximately 400 K the gem-Rh^I-dicarbonyl is reductively agglomerated (see, for example, (4)). This process is inhibited in the presence of NO and it occurs around 500 K, according to the nature of the support (5–7). Here the effect of a $Ce_{0.5}Zr_{0.5}O_2$ mixed oxide upon the dispersion of rhodium particles is analyzed. Evidence is reported that even at very high Rh loading, highly dispersed metal particles can be obtained, which remain highly dispersed after treatments in H_2 or NO/CO atmospheres.

[1] To whom correspondence should be addressed. E-mail: kaspar@univ.trieste.it. Fax: +39 040 6763903.

2. EXPERIMENTAL

2.1. Catalyst Preparation

The $Ce_{0.5}Zr_{0.5}O_2$ mixed oxide was synthesized by a homogeneous gel route from $Ce(acac)_4$ and $Zr(O–Bu)_4$ precursors (Aldrich) according to a previous report (8). It contained about 8% of a CeO_2-rich impurity (8). The support was calcined at 773 K in air for 5 h. The γ-Al_2O_3 was from Alfa Products. Metal impregnation was carried out by the incipient wetness method using a solution of $RhCl_3 \cdot nH_2O$ to obtain an Rh nominal loading of 5 wt%. The catalyst was dried at 393 K overnight and calcined at 773 K for 5 h.

2.2. Volumetric Adsorption Experiments

H_2 chemisorption and BET surface area measurements were conducted using a Micromeritics ASAP 2000 analyzer. In the chemisorption experiments, the samples (ca. 1.0 g) were first reduced in a flow of H_2 (25 ml min^{-1}) at a heating rate of 10 K min^{-1} up to the selected temperature (473 and 773 K). After 2 h at this temperature, the samples were evacuated at 673 K for 5 h and cooled under vacuum to the adsorption temperature (193 K). Typically, an equilibration time of 10 min was employed. Adsorbed volumes were determined by extrapolation to zero pressure of the linear part of the adsorption isotherm. A chemisorption stoichiometry H : Rh = 1 : 1 was assumed.

0021-9517/00 $35.00

2.3. In Situ EXAFS Characterization

Experimental data were recorded in transmission mode at LURE (Orsay, France) using an EXAFS-III line installed on a DCI storage ring, operating at the energy of 1.85 GeV with a typical stored current of 300 mA; a double-crystal monochromator (Si 311), in connection with two ionization chambers filled with argon, was used; at least four spectra were collected for each sample in the energy interval 23050–24100 eV with steps of 2 eV; each point was counted for 2 s.

$Rh/Ce_{0.5}Zr_{0.5}O_2$, in the form of powder, was loaded in a BN holder and mounted in an *in situ* EXAFS cell.[2] Sample weight was adjusted in order to obtain approximately a 2.5 total absorption coefficient immediately after the Rh K-edge. Please note that the Rh K-edge jump obtained under our experimental conditions was only 0.2. All spectra were collected at room temperature (RT), keeping the sample in a controlled atmosphere as described below.

The sample was submitted to the following treatments:

1. The sample was degassed in He (10 ml min^{-1}) for 0.5 h at RT and then measured (FRESH sample).
2. It was reduced for 2 h under H_2 (10 ml min^{-1}) from RT up to 473 K (5 K min^{-1}) and then cooled down under hydrogen to RT, where the spectra were collected (LTR sample).
3. The sample was degassed in He for 0.5 h up to 473 K (5 K min^{-1}) and then treated in a CO (1%)/NO (1.4%) in He mixture (total flow 8 ml min^{-1}) for 4 h at 473 K. The sample was then cooled to RT under He atmosphere and EXAFS spectra were measured (NC473 sample).
4. The treatments described in step 3 were repeated using a reaction temperature of 523 K (NC523 sample).
5. Finally the sample was reduced at 773 K under the gas-flow conditions used for step 2 with a heating rate of 2.5 K min^{-1} (HTR sample).

EXAFS spectra of Rh metal foil, Rh_2O_3, and $RhCl_3$ were measured at RT as standards of known crystallographic structure.

2.4. EXAFS Data Analysis

We performed the analysis using the Fourier filtering method (FFT) with the package written by A. Michalowicz "EXAFS pour le Mac" and experimental standards to obtain accurate data on the first Rh-neighbor shell (9). The EXAFS spectra were extracted from experimental data using the AUTOBK program on the mean absorption spectrum (10). Spectra were k^3-weighted and the Fourier transforms were performed in the interval (2–12 $Å^{-1}$) using a Kaiser window ($\tau = 2.5$); the main peak was filtered and reconstructed using experimental phases and amplitudes deduced from standard compounds. The following known crystallographic reference structures were used, in terms of number of first neighbors (CN) and interatomic distances (R): Rh metal, CN = 12, $R = 2.69$ Å; Rh_2O_3, CN = 6 (oxygen atoms), average $R = 2.05$ Å (3 at 2.03 Å and 3 at 2.07 Å); $RhCl_3$, CN = 6 (chlorine atoms), $R = 2.30$ Å. A value of 0.07 was used for the Debye–Waller (σ) term in the amplitude calculation for the above samples, so the reported σ values for all the samples have a relative meaning.

[2] A full description of the *in situ* EXAFS cell can be found at http://www.dsch.univ.trieste.it/~crevatin/exafs/index.html.

2.5. TEM Studies

Electron micrographs of $Rh/Ce_{0.5}Zr_{0.5}O_2$, Rh/Al_2O_3 (both reduced at 773 K, HTR) and, for the sake of comparison, bare $Ce_{0.5}Zr_{0.5}O_2$ were obtained with a Jeol 2000EX microscope equipped with polar piece and top entry stage. Before the introduction in the instrument, the samples, in the form of powders, were ultrasonically dispersed in isopropyl alcohol, and a drop of the suspension was deposited on a copper grid covered with a lacey carbon film. The histograms of the metal particle size distribution for the HTR $Rh/Ce_{0.5}Zr_{0.5}O_2$ and Rh/Al_2O_3 samples were obtained by counting onto the micrographs at least 300 particles. The mean particle diameter (d_m) was calculated by using the formula $d_m = \sum d_i n_i / \sum n_i$, where n_i was the number of particles of diameter d_i. The counting was carried out on electron micrographs taken at 200,000 magnification, and the observed particles were arranged by classes differing by 0.5 nm in size.

3. RESULTS

3.1. Hydrogen Chemisorption and Textural Properties

Fresh $Rh/Ce_{0.5}Zr_{0.5}O_2$ features a relatively high BET surface area of 86 $m^2\,g^{-1}$ as detected by N_2 adsorption at 77 K. Rh/Al_2O_3 features a BET surface area of 99 $m^2\,g^{-1}$, which is comparable to the value measured on the $Ce_{0.5}Zr_{0.5}O_2$–containing sample.

The hydrogen chemisorption measurements were conducted at 193 K. In fact, at higher temperatures hydrogen spillover from the metal to the ceria–zirconia support may be effective (11, 12). At 193 K, spillover is effectively arrested and the measured H/Rh ratios reflect the metal dispersion as, in that case, hydrogen should be Rh-adsorbed only. Notice that the use of Cl-containing precursors intrinsically hinders hydrogen spillover, since traces of residual chloride would act as an efficient hydrogen spillover killer (13). Despite the high rhodium loading, the H/Rh ratio after reduction of the sample at 473 K is 0.86, indicating a high metal dispersion. After reduction at 773 K, the H/Rh ratio decreases to 0.78, suggesting a very limited sintering of metal particles and/or some particle encapsulation due to loss of surface area. In fact, the total surface area decreased to 65 $m^2\,g^{-1}$ after this treatment, which is somewhat

TABLE 1

Results of Volumetric H_2 Chemisorption and BET Surface Areas Obtained on $Rh/Ce_{0.5}Zr_{0.5}O_2$ and Rh/Al_2O_3[a]

Reduction temp. (K)	Rh surface area ($m^2\ g^{-1}$)	H/Rh_{tot} (%)	Calculated particle size (nm)[b]	BET surface area ($m^2\ g^{-1}$)
473	17.5	0.86	1.3	86
473[c]	10.0	0.45	2.3	99
773	17.1	0.78	1.4	65
773[c]	10.4	0.47	2.2	89

[a] Consecutive experiments; catalyst evacuated at 673 K for 4 h before chemisorption measurement, H_2 adsorption isotherms measured at 193 K.
[b] Calculated assuming a spherical geometry of Rh particles.
[c] Catalyst Rh/Al_2O_3.

lower than that of the fresh sample. The comparison with Rh/Al_2O_3 (Table 1) clearly indicates that under identical catalyst preparation conditions, high dispersion may be obtained when $Ce_{0.5}Zr_{0.5}O_2$ is employed. In fact the H/Rh ratio measured on LTR Rh/Al_2O_3 (H/Rh = 0.45) is nearly half that of LTR $Rh/Ce_{0.5}Zr_{0.5}O_2$ (H/R = 0.86), resulting in a significant difference in the calculated Rh particle size for the two samples (2.3 and 1.3 nm, respectively). Notice that both supports have a similar BET surface areas indicating that the variation of the dispersion should be related to the chemical nature of the support, rather than to a physical effect. After reduction at 773 K the ratio H/Rh of the Rh/Al_2O_3 remains constant, even if some decrease of surface area occurred.

3.2. *EXAFS Analysis*

All the data concerning the results of the fitting EXAFS data are reported in Table 2. Figure 1 reports the EXAFS signals and moduli of Fourier transform (FT) for the $RhCl_3$, Rh_2O_3, $Rh/Ce_{0.5}Zr_{0.5}O_2$-FRESH, NC473, and NC523 samples. A visual inspection of Fig. 1 suggests the absence of

TABLE 2

Results of the Fitting of the EXAFS Signal at the Rh K-edge of the $Rh/Ce_{0.5}Zr_{0.5}O_2$ Samples: Effects of Pretreatments[a]

Sample[a]	CN (and type of atoms)	R (Å)	σ (Å)	ΔE (eV)	N_{ind}	N_{fit}
FRESH	6.3 (O)	2.05	0.097	1.5	9	4
LTR	1.1 (O)	2.13	0.134	6.5	11	8
	5.3 (Rh)	2.69	0.096	−1.0		
NC473	5.5 (O)	2.08	0.131	3.7	9	8
	1.2 (Rh)	2.67	0.116	−5.0		
NC523	5.4 (O)	2.08	0.117	6.4	9	8
	1.0 (Rh)	2.69	0.082	0.0		
HTR	5.4 (Rh)	2.68	0.079	−1.0	10	4

[a] For sample denomination and pretreatment, see Experimental.

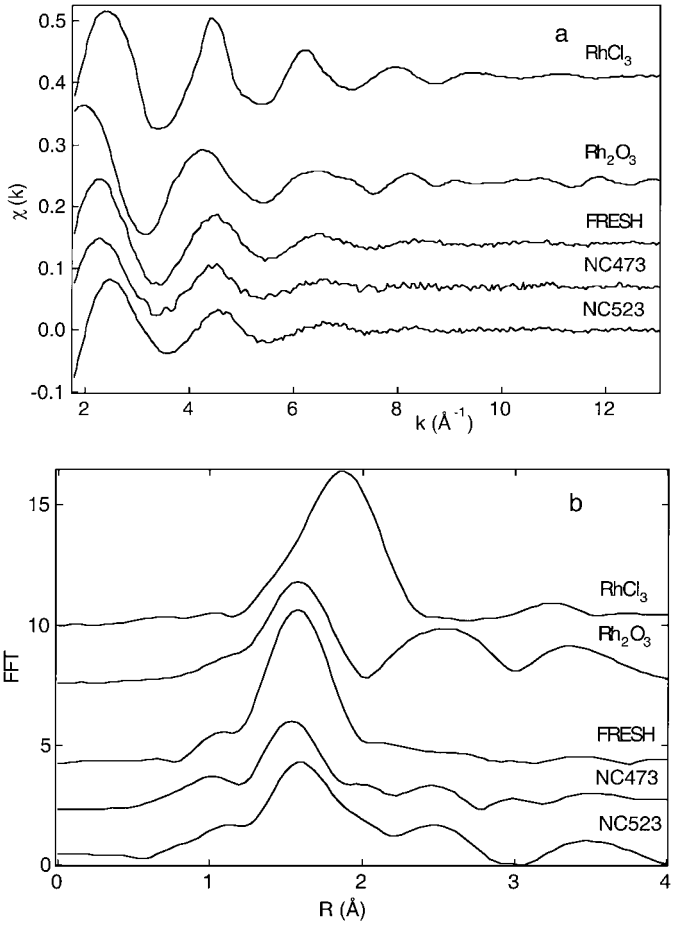

FIG. 1. Experimental EXAFS spectra measured at the Rh K-edge (a) and moduli of the Fourier transform (FT) of the experimental data (R space) (b) of $RhCl_3$, Rh_2O_3, $Rh/Ce_{0.5}Zr_{0.5}O_2$-FRESH, NC473, and NC523 samples. Note that the signals obtained for $RhCl_3$ and Rh_2O_3 are divided by two.

Cl atoms around Rh in all samples, except for the standard $RhCl_3$. In fact the position of the first peak (Cl contribution) in the FT of this compound is clearly shifted to high R compared to the Rh_2O_3 (O contribution). Notice the position of the first peak in the FT of the FRESH, NC473, and NC523, which is very close to that of the Rh_2O_3. This fact will be commented on below.

Figures 2a and 2b report, respectively, EXAFS signals and moduli of FT for Rh metal, LTR, and HTR samples. The fits were performed using the minimization capabilities of the MINUIT program (14); the number of fitting parameters N_{fit} was always smaller than the number of independent points N_{ind}, calculated on the basis of the formula (15)

$$N_{ind} = \frac{2\Delta R \Delta k}{\pi} + 2,$$

where ΔR is the inverse FT interval from R to k space and Δk is the actual interval where the fit is performed.

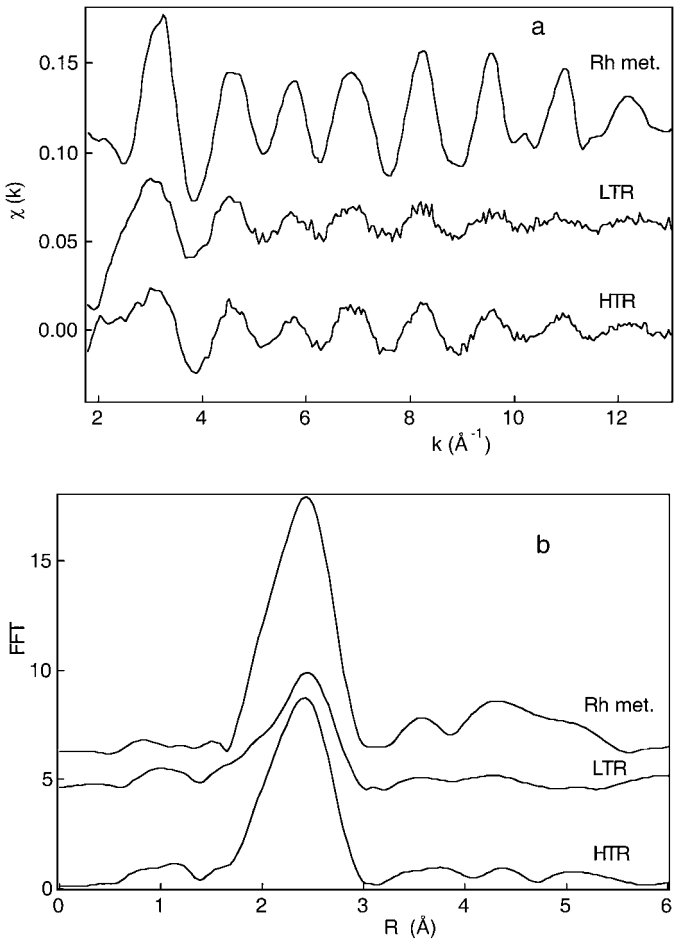

FIG. 2. Experimental EXAFS spectra measured at the Rh K-edge (a) and moduli of the Fourier transform (FT) of the experimental data (*R* space) (b) of Rh metal, LTR, and HTR samples. Note that the signal obtained for Rh metal is divided by two.

The fit of the first peak filter of the FRESH sample (0.82–2.16 Å) is shown in Fig. 3; the numerical results are reported in Table 2. We tried to add a contribution of chlorine atoms but no reliable fitting which includes such contribution could be obtained. This indicates that no detectable chlorine neighbors are present in the first shell of Rh after the initial calcination of the as-prepared sample.

The filtered signal (1.46–3.02 Å) obtained after the first reduction step (LTR sample) shows a typical shape due to the presence of heavy atoms as neighbors (see Fig. 4); nevertheless a reconstruction with only Rh neighbors was unsatisfactory. Addition of an oxygen contribution proved necessary to obtain reasonable fitting, but the Debye–Waller term for oxygen is very high, suggesting a broad distribution of distances (Table 2). Modeling of the signal using two oxygen shells did not improve the fitting appreciably. The overall picture of this sample indicates that reduction at 473 K leads to highly dispersed Rh particles in a close interaction with the support, which are partly oxidized. Notice,

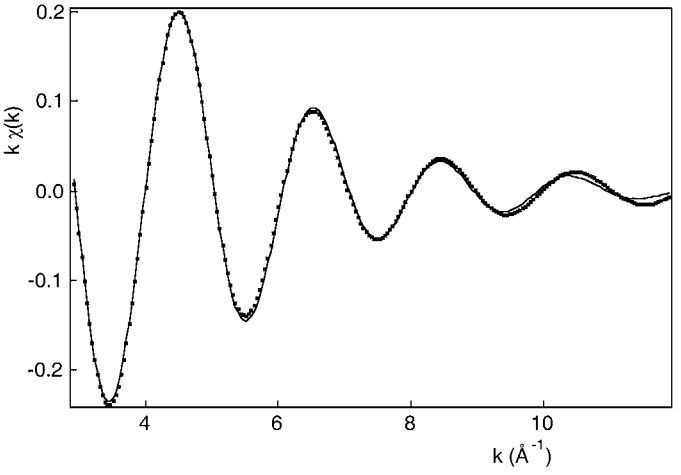

FIG. 3. Back-FT of the first peak and the corresponding fit at the Rh K-edge of FRESH $Rh/Ce_{0.5}Zr_{0.5}O_2$: (■) experimental, (—) fit.

however, that the Rh–Rh bond length is close to that of the metal, indicating that on average the oxidation state of Rh should be close to zero. The analysis of the sample after the NO + CO treatment at 473 K (NC473 sample), disclosed that under reaction conditions Rh particles undergo an oxidative disruption leading to a further fragmentation of the metal clusters. Consistently, the CN of Rh-neighbors is about 1, indicating that oxidative disruption induced by the presence of the two reactants has occurred (3, 7). The fit of the 1.23–2.80 Å region is reported in Fig. 5.

The effect of heating NC743 under reaction conditions at 523 K, in the presence of NO and CO, did not change the EXAFS spectra to a measurable extent. Both NC473 and NC523 samples appear virtually identical, even though it should be mentioned that the quality of the fit for these two

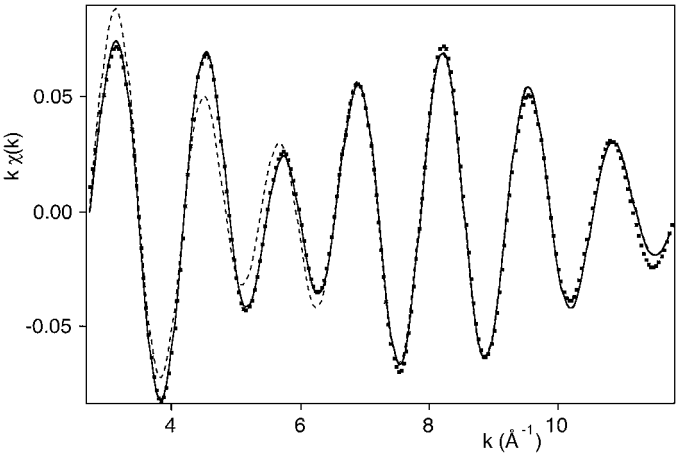

FIG. 4. Back-FT of the first peak and the corresponding fit at the Rh K-edge of LTR $Rh/Ce_{0.5}Zr_{0.5}O_2$: (■) experimental, (---) fit with Rh neighbors, (—) fit with Rh and O neighbors.

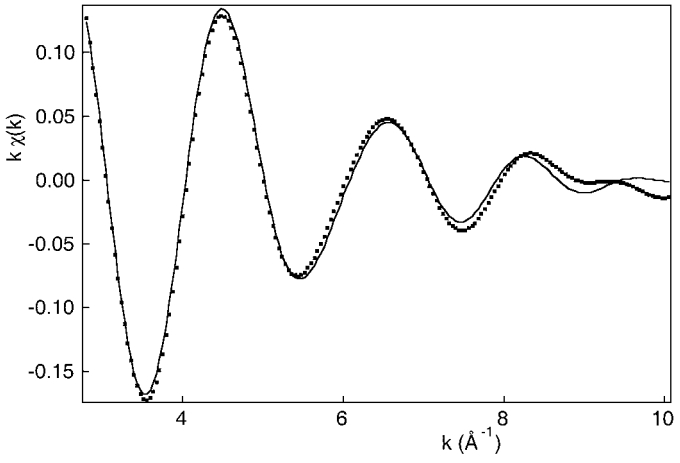

FIG. 5. Back-FT of the first peak and the corresponding fit at the Rh K-edge of NC473 Rh/$Ce_{0.5}Zr_{0.5}O_2$: (■) experimental, (—) fit.

treatments is poorer than for the other cases. Moreover, the σ values indicate the presence of a strong structural disorder.

The reduction process at 773 K re-forms small Rh clusters on the support surface; however, the degree of reduction of the sample seems higher compared to that of the LTR, since all attempts to introduce an oxygen contribution to the EXAFS signal failed. Fitting parameters for the added oxygen were physically inconsistent, and an *F*-test (16) applied to the residual values did not allow us to discriminate between the two models. The fit of the 1.68–3.07 Å region is reported in Fig. 6.

Cube–octahedron symmetry has been inferred from HREM studies as the preferred geometry of the Rh particles supported on CeO_2 (17). Given the high dispersion and the absence of other types of neighbors, we tried to model the Rh particles as small clusters of 13 atoms. Therefore, using the FEFF 7.0 program (18), we have modeled the EXAFS signal by assuming that the cube–octahedron (19) is formed by one rhodium central atom surrounded by twelve first neighbors at the distance of 2.69 with a Debye–Waller term of $\sigma^2 = 0.07$ Å^2. For this model the average CN and bond distances are 5.5 atoms at 2.69 Å, 1.7 at 3.80 Å, 3.7 at 4.66 Å, and 0.9 at 5.38 Å. A particle size of 8.1 Å is calculated for this cluster. As suggested by a referee, other cluster geometries were tested, such as decahedron and icosahedron ones. Figure 7 reports the FTs of the calculated signals compared to the experimental FT. Even if there is an approximation in our models, since Rh–Rh distances are kept constant with respect to the metal and an average $\sigma^2 = 0.007$ Å^2 was assumed, a perusal of Fig. 7 reveals that only a cube–octahedral model can reasonably reproduce the experimental signal. Notice the zone indicated by the arrows in Fig. 7. Accordingly, we suggest that the rhodium clusters are present mainly in the form of 13-atom clusters, indicating a remarkably high dispersion of the Rh metal.

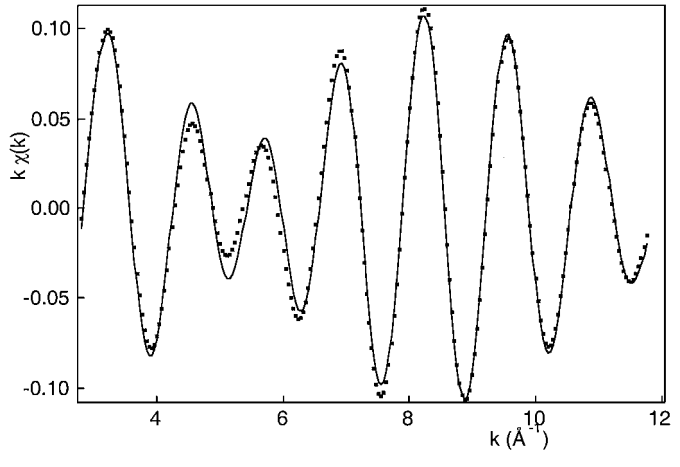

FIG. 6. Back-FT of the first peak and the corresponding fit at the Rh K-edge of HTR Rh/$Ce_{0.5}Zr_{0.5}O_2$: (■) experimental, (—) fit.

Due to the small size of the Rh clusters, an asymmetric distribution could be expected, as reported in other studies on small clusters (20). We therefore used the cumulants expansion series up to the fourth term and performed the calculations with Feffit 2.32× (21) and FEFF 7.0 (18) codes. Both third and fourth cumulants were close to zero, suggesting that no correction to the Gaussian distribution was necessary to model the signal of the first neighbor of Rh.

3.3. HREM Analysis

The TEM image of the HTR Rh/$Ce_{0.5}Zr_{0.5}O_2$ shows very small particles, well distributed onto larger micro-crystals (Fig. 8, top). Such features are absent in electron micrographs of the bare support taken at the same magnification and with similar focus conditions, so they can be attributed to Rh bearing clusters. In fact, a separated temperature-programmed oxidation experiment showed that adsorbed carbon species, which could interfere in the particle size analysis, are practically absent in the system. A statistical analysis of the dimension of these particles resulted in a very narrow size distribution with mean diameter $d_m = 1.2$ nm (Fig. 9). This result is in good agreement with the mean metal particle diameter provided by analysis of EXAFS data and H_2 chemisorption measurements (Table 1). However, it must be noticed that the HTR sample was re-exposed to air before introduction to the microscope. As a consequence some re-oxidation of the system could occur under these conditions, and therefore partly oxidized Rh-supported particles could be observed by TEM instead of metallic Rh clusters.

The comparison with the results obtained on the Rh/Al_2O_3 is striking (Fig. 8, bottom). In this case large

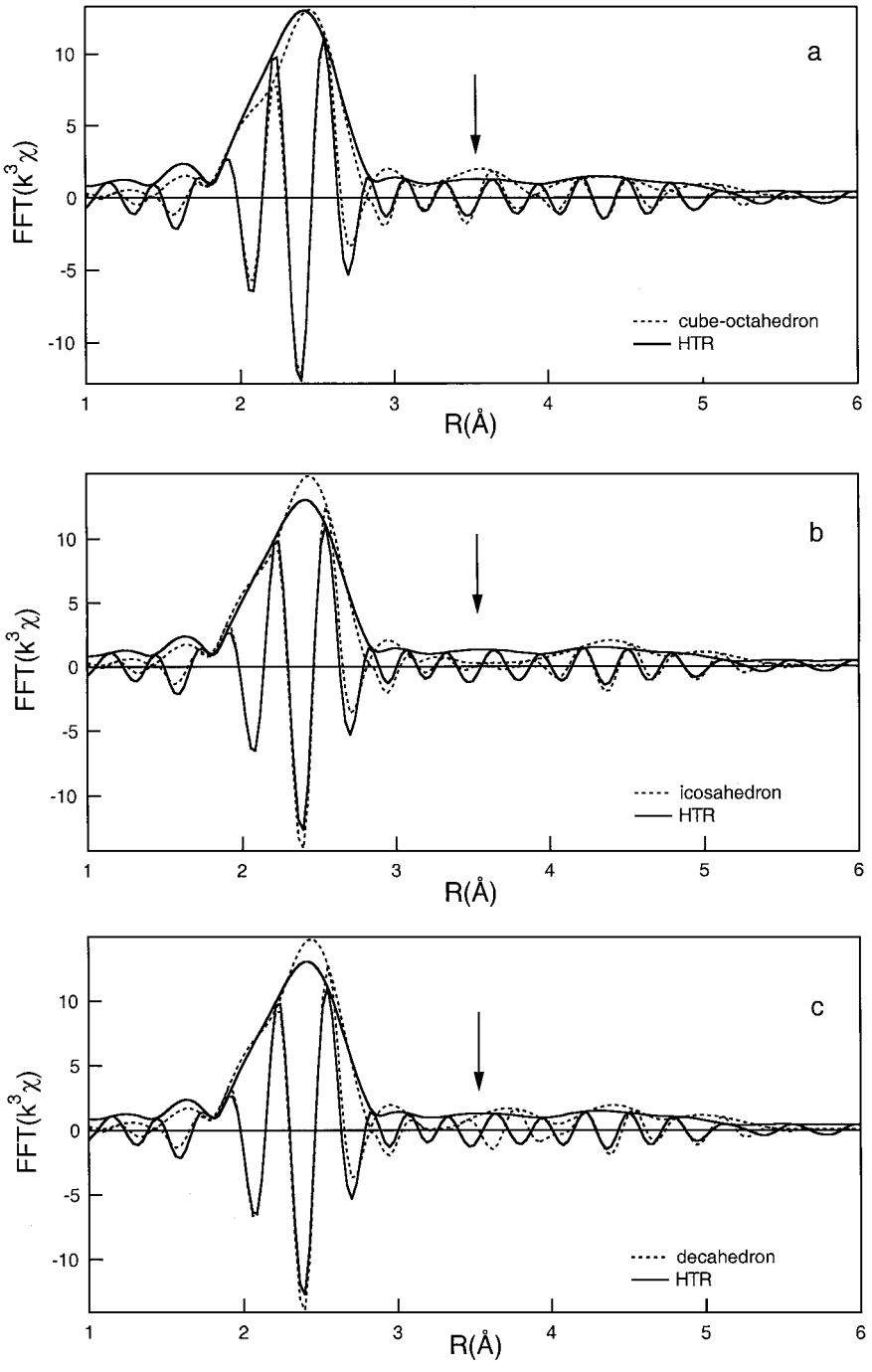

FIG. 7. Comparison of moduli and the imaginary part of the FT of the experimental data at the Rh K-edge of HTR $Rh/Ce_{0.5}Zr_{0.5}O_2$ and the corresponding modelled data using Rh particle models: (a) cube–octahedron, (b) icosahedron, (c) decahedron, (---) experimental, (—) model.

supported particles, easily distinguishable from the support, are present. Their size is distributed over a broad range (1–6 nm), with a significant fraction of particles as large as 6 nm, while particles smaller than 0.5 nm are absent (Fig. 9). The average particle diameter is about twice that of HTR $Rh/Ce_{0.5}Zr_{0.5}O_2$, again in a good agreement with the value calculated from the H_2 chemisorption results (Table 1).

4. DISCUSSION

Addition of ZrO_2 to the NM/CeO_2 catalysts with formation of a CeO_2–ZrO_2 solid solution has represented a major improvement in TWCs in the 1990s and has been thought to contribute mainly to their high oxygen capacity and thermal stability (1). Recent work, however, disclosed that other effects seem to be present in these materials; in particular,

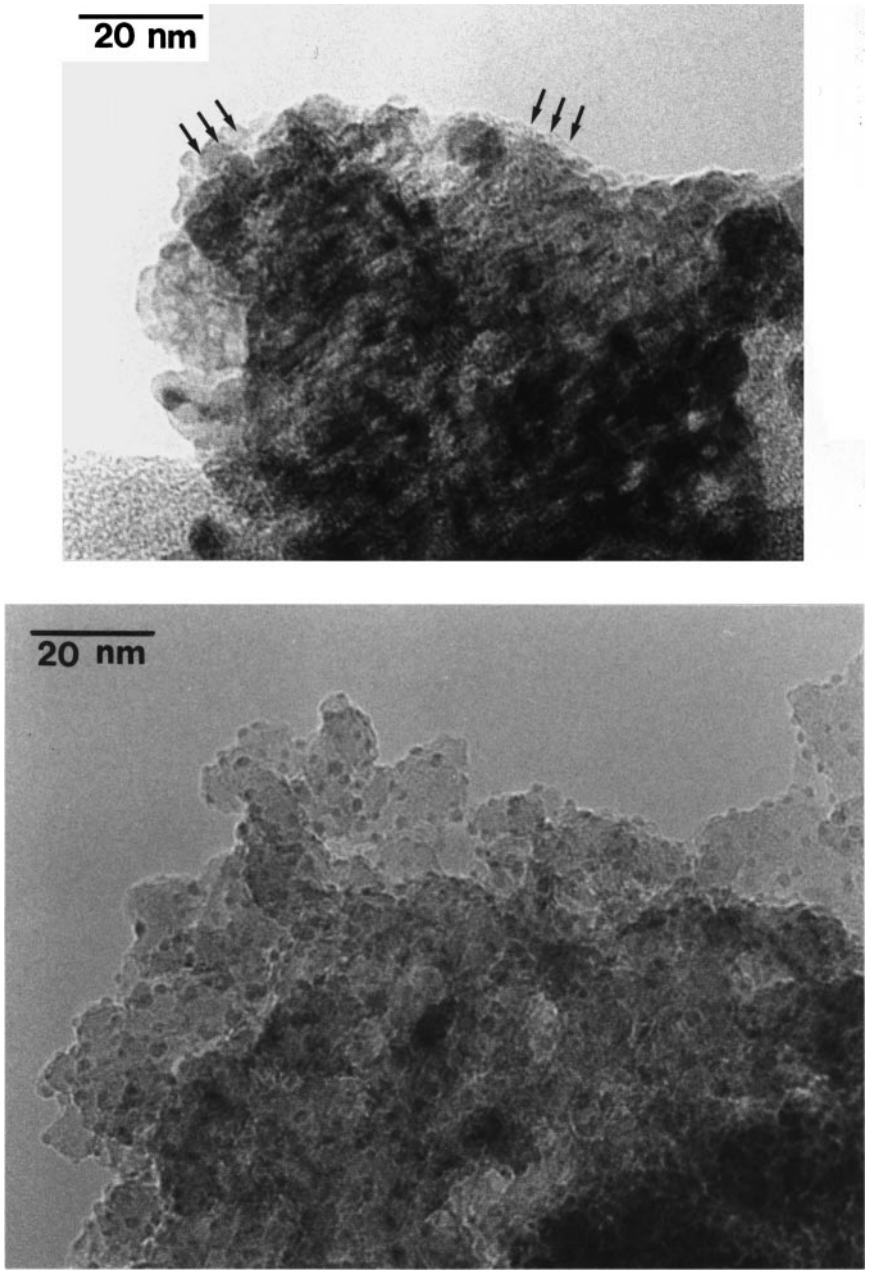

FIG. 8. TEM images of HTR $Rh/Ce_{0.5}Zr_{0.5}O_2$ (top) and HTR Rh/Al_2O_3 (bottom).

CeO_2–ZrO_2 mixed oxides were suggested to promote the NO reduction using CO as reductant (3). It was also shown that the CeO_2–ZrO_2 support stabilizes the presence of Rh^+ species under $NO/CO/O_2$ mixture under the reaction conditions (22). On the other hand, it is well known that Rh particles easily undergo in the presence of CO an oxidative disruption to give Rh(I) species. The reverse process, e.g., reductive agglomeration of Rh(I) species, is promoted by CO at high temperatures. When Rh is supported on Al_2O_3 the latter process occurred at 500 K (7), while it was not observed up to 523 K in $Rh/Ce_{0.5}Zr_{0.5}O_2$.

The present data clearly shows that despite the comparable surface areas of the two supports employed—it is somewhat higher in the Al_2O_3 sample—and the same preparation methodology, the dispersion of Rh is greatly enhanced in $Rh/Ce_{0.5}Zr_{0.5}O_2$ compared to Rh/Al_2O_3. In fact, in the fresh samples, we observed that H/Rh is almost double in the former catalyst. All the techniques employed here clearly indicate that very high dispersion and uniform distribution of the Rh particles centered around 1 nm are obtained using the $Ce_{0.5}Zr_{0.5}O_2$ support, and they are retained even after reduction at 773 K. It is worth

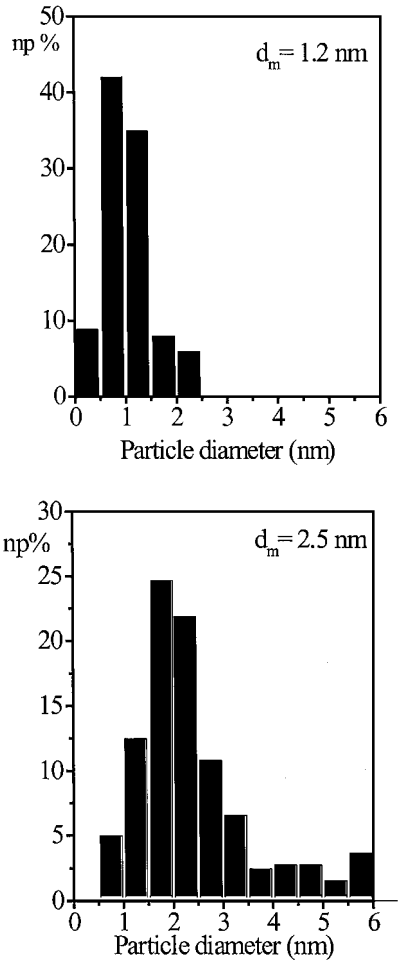

FIG. 9. Supported particle size distribution for the HTR $Rh/Ce_{0.5}Zr_{0.5}O_2$ ($d_m = 1.2$ nm) and HTR Rh/Al_2O_3 ($d_m = 2.5$ mm) samples.

noting that the presence of cube–octahedron metal clusters of similar dimension have been inferred for an industrial Pt/Al_2O_3 catalyst at metal loadings below 0.6 wt% (19). We guess that the presence of the CeO_2-based support is able to stabilize the Rh dispersion in a way similar to that observed for CeO_2, which is known to promote NM–O–Ce interaction, leading to stabilization of the metal dispersion.

In agreement with this interpretation, we detected by the *in situ* EXAFS measurements oxidized rhodium species under reaction conditions, which do not undergo the reductive agglomeration. This might be an indirect indication that the above-reported type of interaction might be present in our system.

Another interesting observation is that Cl has not been detected by EXAFS around the Rh center in any of the samples investigated. This is rather remarkable, keeping in mind that chloride is generally rather difficult to remove. This result suggests that chloride, although not detected, could be located essentially on the support. Cerium oxychloride species have indeed often been detected in the CeO_2-based catalyst prepared from chloride-containing precursors, and they were shown to posses high thermal stability (23, 24).

In summary, we have shown that use of $Ce_{0.5}Zr_{0.5}O_2$ as a support favors high dispersion of Rh particles with a rather narrow distribution of particle sizes, a 13-atom cluster being suggested as mainly present on the mixed oxide surface. The particle morphology is hardly affected by reduction at 473–773 K. In contrast, in the presence of NO and CO, Rh particles are easily oxidized and further disrupted. Finally, conditions for H_2 chemisorption are reported which should give reliable measurements of the Rh dispersion in the Rh/CeO_2–ZrO_2 catalysts. Work is in progress on this point.

ACKNOWLEDGMENTS

Mr. Elvio Merlach and Mr. Renzo Crevatin, Dipartimento di Scienze Chimiche, Università di Trieste, are gratefully acknowledged for the design and manufacture of the *in situ* EXAFS cell. The University of Trieste, the Ministero dell'Ambiente (Roma), Contract DG 164/SCOC/97, CNR (Roma) Programmi Finalizzati "Materiali Speciali per Tecnologie Avanzate II, Contract 97.00896.34, and MURST (Roma) "Progetti di Ricerca di Rilevante Interesse Nazionale—1998" are gratefully acknowledged for financial support. The technical assistance of the staff at LURE is gratefully acknowledged.

REFERENCES

1. Kašpar, J., Fornasiero, P., and Graziani, M., *Catal. Today* **50**, 285 (1999).
2. Trovarelli, A., *Catal. Rev. Sci. Eng.* **38**, 439 (1996).
3. Fornasiero, P., Ranga Rao, G., Kašpar, J., L'Erario, F., and Graziani, M., *J. Catal.* **175**, 269 (1998).
4. Solymosi, F., and Pasztor, M., *J. Phys. Chem.* **89**, 4789 (1985).
5. Solymosi, F., Bansagi, T., and Novak, E., *J. Catal.* **112**, 183 (1988).
6. Novak, E., Sprinceana, D., and Solymosi, F., *Appl. Catal. A. Gen.* **149**, 89 (1997).
7. Kašpar, J., de Leitenburg, C., Fornasiero, P., Trovarelli, A., and Graziani, M., *J. Catal.* **146**, 136 (1994).
8. Fornasiero, P., Balducci, G., Di Monte, R., Kašpar, J., Sergo, V., Gubitosa, G., Ferrero, A., and Graziani, M., *J. Catal.* **164**, 173 (1996).
9. Michalowicz, A., "Logiciel pour la Chimie," p.751. Societé Francaise de Chimie, Paris, 1991.
10. Newville, M., Livins, P., Yacoby, Y., Rehr, J. J., and Stern, E. A., *Phys. Rev. B* **47**, 14126 (1993).
11. Bernal, S., Botana, F. J., Calvino, J. J., Cauqui, M. A., Cifredo, G. A., Jobacho, A., Pintado, J. M., and Rodriguez-Izquierdo, J. M., *J. Phys. Chem.* **97**, 4118 (1993).
12. Fornasiero, P., Kašpar, J., and Graziani, M., *J. Catal.* **167**, 576 (1997).
13. Martin, D., and Duprez, D., *J. Phys. Chem. B* **101**, 4428 (1997).
14. James, F., and Roos, H., *Comput. Phys. Commun.* **10**, 343 (1975).

15. Stern, E. A., *Phys. Rev. B* **48**, 9825 (1993).
16. Joyner, R. W., Martin, K. J., and Meehan, P., *J. Phys. C Solid State Phys.* **20**, 4005 (1987).
17. Bernal, S., Calvino, J. J., Cauqui, M. A., Gatica, J. M., Larese, C., Omil, J. A. P., and Pintado, J. M., *Catal. Today* **50**, 175 (1999).
18. Ankunidov, A., Ravel, B., Rehr, J. J., and Conradson, S., *Phys. Rev. B* **58**, 7565 (1998).
19. Lagarde, P., Murata, T., Vlaic, G., Freund, E., Dexpert, H., and Bournonville, J., *J. Catal.* **84**, 333 (1983).
20. Clausen, B. S., Graabaek, L., Topsoe, H., Hausen, L. B., Stolze, P., Norskov, J. K., and Nielsen, O. H., *J. Catal.* **141**, 368 (1993).
21. Newville, M., Ravel, B., Haskel, D., Stern, E. A., and Yacoby, Y., *Physica B* **208/209**, 154 (1995).
22. Fajardie, F., Tempere, J. F., Manoli, J. M., Touret, O., Blanchard, F., and Djega-Mariadassou, G., *J. Catal.* **179**, 469 (1998).
23. Kondarides, D. I., and Verykios, X. E., *J. Catal.* **174**, 52 (1998).
24. Fajardie, F., Tempere, J. F., Manoli, J. M., Djega-Mariadassou, G., and Blanchard, G., *J. Chem. Soc. Faraday Trans.* **94**, 3727 (1998).